Fast CZ Gate via Energy-Level Engineering in Superconducting Qubits with a Tunable Coupler

Benzheng Yuan¹,* Chaojie Zhang¹, Chuanbing Han¹, Shuya Wang¹, Peng Xu¹, Huihui Sun¹, Qing Mu¹, Lixin Wang¹, Bo Zhao¹, Weilong Wang¹,[†] and Zheng Shan^{1‡}

¹Laboratory for Advanced Computing and Intelligence Engineering,

Information Engineering University, Zhengzhou 450001, Henan, China

(Dated: October 15, 2025)

In superconducting quantum circuits, decoherence errors in qubits constitute a critical factor limiting quantum gate performance. To mitigate decoherence-induced gate infidelity, rapid implementation of quantum gates is essential. Here we propose a scheme for rapid controlled-Z (CZ) gate implementation through energy-level engineering, which leverages Rabi oscillations between the $|11\rangle$ state and the $(|02\rangle+|20\rangle)/\sqrt{2}$ superposition state in a tunable-coupler architecture. Numerical simulations achieved a 17 ns nonadiabatic CZ gate with fidelity over 99.99%. We further investigated the performance of the CZ gate in the presence of anharmonicity offsets. The results demonstrate that a high-fidelity CZ gate with an error rate below 10^{-4} remains achievable even with finite anharmonicity variations. Furthermore, the detrimental impact of spectator qubits in different quantum states on the fidelity of CZ gate is effectively suppressed by incorporating a tunable coupler. This scheme exhibits potential for extending the circuit execution depth constrained by coherence time limitations.

I. INTRODUCTION

Achieving high-fidelity quantum gates is a critical challenge in the realization of fault-tolerant quantum computation [1, 2]. Decoherence errors constitute the dominant error source in the superconducting quantum processor. To mitigate decoherence errors in superconducting qubits, extensive research has focused on advancing qubit hardware design and material processing techniques [3– 13. On the other hand, rapid gate implementations are essential to suppress decoherence-induced infidelity, and also enable deeper quantum circuits to be executed within the finite coherence times of qubits. These advancements are particularly critical for widely deployed quantum gates such as the CZ gate. Current physical implementations of CZ gates in superconducting circuits can be categorized into two paradigms based on their evolution mechanisms: adiabatic [14–16] and nonadiabatic approaches [17-19]. The adiabatic scheme relies on the cross-Kerr type ZZ interaction between two qubits, achieving phase accumulation on |11\rangle state through parametric modulation. This approach typically employs either frequency tuning of qubits or couplers to achieve phase accumulation [16, 20, 21], or microwave pulsedriven mediation of ZZ interactions [22, 23]. Nonadiabatic CZ gates utilize Rabi oscillations between |11\rangle and either $|02\rangle$ or $|20\rangle$ states [17–19]. In summary, the implementation of CZ gates typically utilizes the interaction between two states within the double excitation mainfold.

To overcome the speed limitations of the conventional CZ gate, we introduce an energy-level engineering strat-

egy designed to enhance the effective qubit-qubit interaction. An enhanced effective coupling strength of 2gis achieved by engineering a resonance between the $|11\rangle$ state and the $(|20\rangle + |02\rangle)/\sqrt{2}$ superposition state, compared to the conventional $\sqrt{2g}$. The resonance condition is satisfied when the energy levels $E_{11} = E_{20} = E_{02}$, enabling high-speed gate operation. This spectral alignment requires a pair of qubits with opposing anharmonicities and a frequency separation equal to the magnitude of the anharmonicity. Although similar spectral conditions have been explored in ZZ-suppression architectures, for example, in hybrid Transmon-CSFQ (capacitively shunted flux qubit) systems [24–26], their practical implementation via direct capacitive coupling is hindered by a fundamental scalability issue: the frequency tuning necessary for gate operation often induces unintended crosstalk with spectator qubits in densely spaced frequency spectra. These unwanted interactions significantly compromise gate fidelity in multi-qubit settings [27, 28]. Consequently, conventional capacitive coupling methods face inherent limitations when extended to oneor two-dimensional qubit arrays.

To address this fundamental constraint while maintaining high-speed gate operation, we introduce a tunable coupler architecture that enables frequency-independent coupling control. The proposed design incorporates a non-resonant pair consisting of a Transmon and an inductively shunted transmon (IST), the latter providing positive anharmonicity at the operating point [29], coupled via a flux-tunable transmon coupler [30]. By leveraging Rabi oscillations between the $|110\rangle$ state and the symmetric superposition state $(|200\rangle + |020\rangle)/\sqrt{2}$, we achieve an enhanced effective Rabi frequency of 2g, thereby reducing the duration of CZ gate to $\pi/(2g)$ with an infidelity below 10^{-4} . To evaluate robustness against fabrication variations, we further investigate the performance of CZ gate under anharmonicity offsets ($\delta \neq 0$). The numerical

^{*} Benzhengyuan@outlook.com

 $^{^\}dagger$ Corresponding Author; wangwl19888@163.com

[‡] Corresponding Author; shanzhengzz@163.com

results confirm that the CZ gate maintains an error rate below 10^{-4} even with finite anharmonicity deviations. Moreover, by incorporating the tunable coupler, the architecture effectively suppresses crosstalk from spectator qubits in arbitrary quantum states, ensuring high fidelity in multi-qubit environments.

The paper is structured as follows: Section II presents a theoretical analysis of the Hamiltonian governing the circuit system. Section III explains the operational principles of rapid CZ gates, elucidating the physical origins of their accelerated operation speeds. Section IV delivers comprehensive numerical results. Finally, the work is summarized in the Section V.

II. PHYSICAL MODEL

Tunable coupling has been demonstrated as a leading physical architecture. We now consider the physical model depicted in Fig. 1(a), which consists of a Transmon and an IST coupled via a tunable coupler. The Hamiltonian of system can be described as:

$$\hat{H}_{s} = \sum_{i=1,c} 4E_{Ci}\hat{n}_{i}^{2} - 2E_{Ji} \left| \cos \left(2\pi \phi_{ext}^{i} \right) \right| \cos \hat{\varphi}_{i}$$

$$+ 4E_{C2}\hat{n}_{2}^{2} - E_{J2} \cos \left(\hat{\varphi}_{2} + 2\pi \phi_{ext}^{2} \right) + \frac{1}{2}E_{L}\hat{\varphi}_{2}^{2}$$

$$+ J_{1c}\hat{n}_{1}\hat{n}_{c} + J_{2c}\hat{n}_{2}\hat{n}_{c} + J_{12}\hat{n}_{1}\hat{n}_{2},$$

$$(1)$$

where the index i=1,2 denotes the Transmon and IST modes, respectively, and c lables the transmon coupler mode. E_C, E_J and E_L represent charging energy, Josephson energy and inductive energy, respectively. ϕ_{ext} is the external flux bias. The IST is working at half-flux quanta $(\phi_{ext}=0.5)$, realizing a single-well plasmonic spectrum with positive anharmonicity $\alpha \geq 0$ (see Appendix A for details).

We approximate the qubits and the coupler as harmonic modes, i.e., introducing $\hat{\varphi}_i = \hat{\varphi}_{i,zpf} \left(\hat{a}_i^{\dagger} + \hat{a}_i \right)$ and $\hat{n}_i = i\hat{n}_{i,zpf} \left(\hat{a}_i^{\dagger} - \hat{a}_i \right)$, where phase (number) zeropoint fluctuation $\hat{n}_{i,zpf} = 1/\left(2\hat{\varphi}_{i,zpf}\right)$. Thus, the system Hamiltonian can be written as follows:

$$\hat{H}/\hbar = \sum_{i=1,2,c} \left(\omega_i \hat{a}_i^{\dagger} \hat{a}_i + \frac{\alpha_i}{2} \hat{a}_i^{\dagger} \hat{a}_i^{\dagger} \hat{a}_i \hat{a}_i \right) + \sum_{i < j} g_{ij} \left(\hat{a}_i^{\dagger} \hat{a}_j + \hat{a}_i \hat{a}_j^{\dagger} \right),$$

$$(2)$$

where \hat{a}_i^{\dagger} and \hat{a}_i are, respectively, the raising and lowering operators truncated to the lowest four levels (labeled as $\{|0\rangle, |1\rangle, |2\rangle, |3\rangle\}$), defined in the eigenbasis of the corresponding oscillators. $g_{ij}(i, j = 1, 2, c)$ denotes the coupling strength. The derivation of the circuit quantization is detailed in Appendix A.

The energy-level structure of each qubit is shown in Fig. 1(b). The Hamiltonian under the rotating-wave approximation (RWA) including levels with two excitations

for the system in Fig. 1(a) can be written as

$$\hat{H} = \begin{bmatrix} \omega_{000} & 0 & 0 & 0 & 0 & 0\\ 0 & \omega_{010} & 0 & g & 0 & 0\\ 0 & 0 & \omega_{020} & 0 & \sqrt{2}g_{12} & 0\\ 0 & g & 0 & \omega_{100} & 0 & 0\\ 0 & 0 & \sqrt{2}g_{12} & 0 & \omega_{110} & \sqrt{2}g_{12}\\ 0 & 0 & 0 & 0 & \sqrt{2}g_{12} & \omega_{200} \end{bmatrix}$$
(3)

in the $\{|000\rangle, |010\rangle, |020\rangle, |100\rangle, |110\rangle, |200\rangle\}$ basis, where the bare state of the system is denoted by $|n_i n_j n_c\rangle = |n_i\rangle \otimes |n_j\rangle \otimes |n_c\rangle (n_i, n_j \in \{0, 1, 2\}, n_c = 0).$

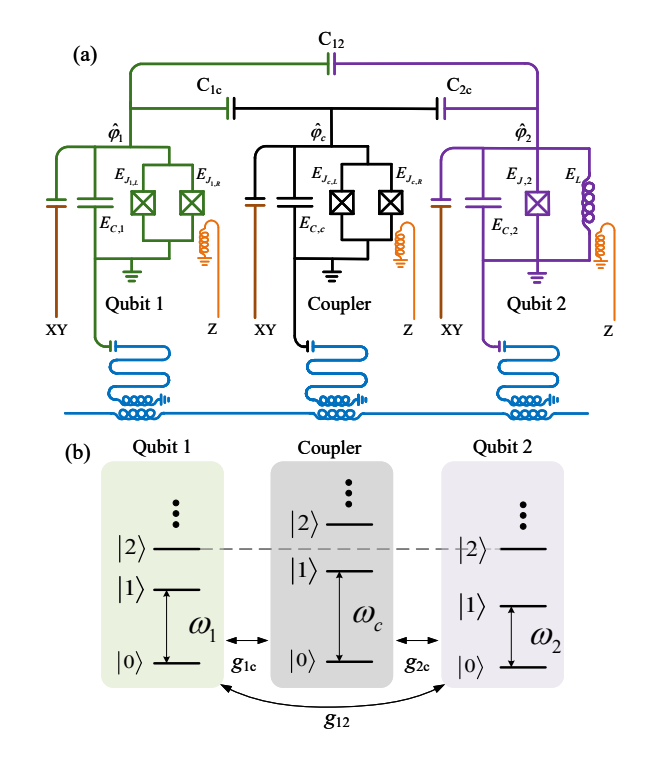


FIG. 1. (a) Schematic of the superconducting circuit featuring a Transmon and an IST qubit coupled via a tunable coupler. (b) Corresponding energy-level diagram demonstrating the condition $E_{110}=E_{200}=E_{020}$ (subscripts denote Q1, Q2, coupler) required for a fast CZ gate. The coupling strengths are denoted by $g_{12}/2\pi=10$ MHz (qubit-qubit) and $g_{ic}/2\pi=100$ MHz (qubit-coupler, i=1,2).

III. FAST CZ GATE

The CZ gate is a fundamental two-qubit phase gate widely used in superconducting quantum circuits. Conventional CZ gate implementations utilize the $|110\rangle-|020\rangle$ or $|110\rangle-|200\rangle$ interactions, with the associated energy-level structures and coupling mechanisms depicted in Fig. 2(a) and Fig. 2(b). Under this configuration, the system Hamiltonian in the rotating frame can be expressed as:

$$H^* = \sqrt{2}g_{12} (|110\rangle \langle 200| + |200\rangle \langle 110|) \tag{4}$$

The resulting evolution, described by the operator $U = \exp(-iH^*t)$, can be visualized on the Bloch sphere as shown in Fig. 2(d). The CZ gate is realized when the evolution time reaches $t = \pi/(\sqrt{2}g_{12})$. It is evident that the gate duration in this scheme is fundamentally limited by the underlying coupling mechanism. To overcome this speed constraint, we now introduce an alternative approach for rapidly implementing the CZ gate through deliberate engineering of the energy-level structure.

To rapidly implement the CZ gate, the parameters of the qubits can be set as $\omega_i + \alpha_i = \omega_j$ $(i,j \in \{1,2\})$, the energy level structure and coupling are shown in Fig. 2(c). The opposite anharmonicity required between the two qubits in this scheme is satisfied through the Transmon-IST coupling configuration described in Section II, with the complete parameter set provided in Table I. Under these parameter conditions, after the rotating frame with transform operator $V = \exp\left[-i(\omega_{200} |200\rangle \langle 200| + \omega_{020} |020\rangle \langle 020| + \omega_{110} |110\rangle \langle 110|)t\right]$. Then Eq. (3) can be written as

$$\hat{H'} = \sqrt{2}g_{12} (|110\rangle \langle 020| + |020\rangle \langle 110|) + \sqrt{2}g_{12} (|110\rangle \langle 200| + |200\rangle \langle 110|)$$
(5)

with the introduction of state $|B\rangle$. The system Hamiltonian becomes

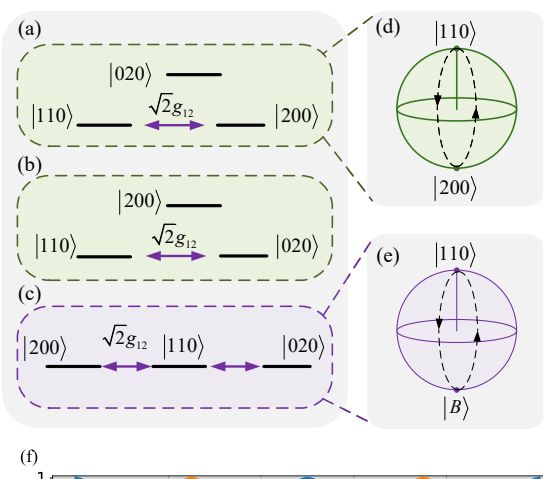
$$\hat{H}' = 2g_{12} (|110\rangle \langle B| + \text{H.c.}),$$
 (6)

where the state $|B\rangle = (|200\rangle + |020\rangle)/\sqrt{2}$. The evolution between the $|110\rangle$ and $|B\rangle$ states, governed by an interaction strength of $2g_{12}$, is illustrated on the Bloch sphere in Fig. 2(e). The enhancement of the coupling strength from $\sqrt{2}g_{12}$ to $2g_{12}$ represents not merely a numerical improvement, but a fundamental optimization of the underlying physical mechanism that directly enables the accelerated performance of the CZ gate.

In the basis $\{|110\rangle, |B\rangle\}$, we can map $(|110\rangle\langle B| + \text{H.c.})$ to Pauli matrix σ_x . Based on this, when the evolution time $t = \pi/2g_{12}$, the $|11\rangle$ state evolves to $-|11\rangle$. The dynamics generated by this Hamiltonian is shown in Fig. 2(f). A coherent oscillation between the $|11\rangle$ state and the $|B\rangle$ state can be realized. A full oscillation cycle completes the phase accumulation required for the CZ gate. In the following, we numerically simulate the performance of this scheme under realistic experimental conditions.

TABLE I. Qubit Parameters for Implementing the Fast CZ Gate. These parameters can be derived from the Hamiltonian in Appendix A.

Qubit	Transmon	IST
Frequency(GHz)	4.50	4.25
Anharmonicity(MHz)	-250	250
$E_L(GHz)$	-	24.5
$E_J(GHz)$	14.0	14.9
$E_C(MHz)$	221	228



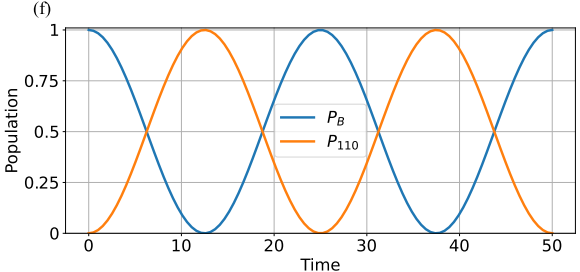


FIG. 2. Mechanisms for conventional and accelerated CZ gate implementation. (a, b) Energy-level diagrams and coupling configurations for conventional CZ gates mediated by the $|110\rangle - |020\rangle$ and $|110\rangle - |200\rangle$ interaction, respectively. (c) Engineered energy-level structure satisfying $\omega_i + \alpha_i = \omega_j \ (i,j \in \{1,2\})$. (d) Bloch sphere representation of the state evolution under conventional couplings. (e) Bloch sphere representation of the state evolution between $|110\rangle$ and $|B\rangle = (|200\rangle + |020\rangle)/\sqrt{2}$. (f) Coherent oscillation between $|110\rangle$ and $|B\rangle$ under the effective Hamiltonian.

IV. PERFORMANCE OF CZ GATE

To evaluate the performance of rapid CZ gates in this architecture, we calculate the average gate fidelity using the standardized metric [31],

$$\overline{F} = \frac{\left| \operatorname{Tr} \left(\hat{U}_{id}^{\dagger} \hat{U} \right) \right|^{2} + \operatorname{Tr} \left(\hat{U}^{\dagger} \hat{U} \right)}{d(d+1)}, \tag{7}$$

where $d=2^n$ for an n-qubit system, \hat{U}_{id} represents the ideal unitary operation, and \hat{U} denotes the numerically simulated operation. All numerical simulations are performed using the QuTiP (Quantum Toolbox in Python) package [32].

The main idea of implementing the CZ gate is as follows. In practical circuit design, the qubit frequencies and anharmonicity can be engineered such that $\omega_i + \alpha_i = \omega_j$ $(i, j \in \{1, 2\})$. Under ideal conditions (assuming ideal fabrication conditions), the qubit frequencies can be set using fixed-frequency qubits to satisfy the energy-level requirement. However, considering the frequency drift and fabrication variability inherent, one

Transmon is designed to be frequency tunable. By simultaneously adjusting the frequencies of both the coupler and the Transmon from their respective idle points (ω_c^{off} and ω_a^{off}) to their working points, according to the time-dependent pulse function as shown in Fig. 3(a). The interqubit coupling $|110\rangle \leftrightarrow |B\rangle$ can be activated, enabling a fast CZ gate.

The frequency pulse profile that we use throughout this work is

$$\omega_{i}(t) = \omega_{\text{off}} + \frac{\omega_{\text{on}} - \omega_{\text{off}}}{2} \left[\text{Erf}\left(\frac{t - \frac{1}{2}t_{\text{ramp}}}{\sqrt{2}\sigma}\right) - \text{Erf}\left(\frac{t - t_{\text{gate}} + \frac{1}{2}t_{\text{ramp}}}{\sqrt{2}\sigma}\right) \right], \tag{8}$$

where $\omega_{\rm off}$ and $\omega_{\rm on}$ denote the frequency of the qubit/coupler at the parking point and the interaction point. $t_{\rm ramp} = 4\sqrt{2}\sigma$ is the ramp time, $t_{\rm gate}$ denotes the total gate time for the CZ gate. $t_{\text{hold}} = t_{\text{gate}} - t_{\text{ramp}}$ denotes the hold time that is defined as the time interval between the midpoints of the ramps. By simultaneously optimizing the operating frequencies of the coupler ω_{on}^c and the qubit $\omega_{\text{on}}^{\hat{q}}$ with the pulse sequence illustrated in Fig. 3(a) and initializing the system in states $|11\rangle'$ and $|01\rangle'$, we calculate the leakage error, defined as $\varepsilon_{leak} = 1 - P_{11}$, and the swap error, defined as $\varepsilon_{\text{swap}} = 1 - P_{01}$, as a function of the hold time. Here, P_{ij} denotes the population in the state $|ij\rangle$, although the label omits the coupler; the full physical system is a three-mode system that includes it. The gate operation is optimized to minimize leakage, which demonstrates that a CZ gate with fidelity exceeding 99.99% can be achieved within a hold time of 17 ns, while the leakage and swap errors are suppressed below 10^{-4} , as show in Fig. 3(b).

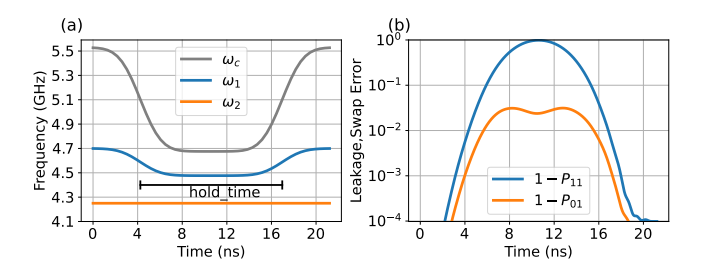


FIG. 3. (a) Frequency pulse scheme for realizing a fast CZ gate by simultaneously tuning the frequencies of the Transmon and the coupler to shift the system from the idle point to the work point. The anharmonicities are set as $-\alpha_1=\alpha_2=2\pi\times250$ MHz. (b) Simulated leakage and swap errors of the fast CZ gate as functions of the control parameters defined in (a).

We further examined the effect of asymmetric anharmonicity, defined by the offset error $\delta = |\alpha_1| - |\alpha_2|$. As shown in Fig. 4, even with substantial asymmetry, such as $\delta/2\pi = 10$ MHz and 20 MHz, a CZ gate fidelity above 99.99% remains achievable through optimized pulse shaping, with both leakage and swap errors consistently suppressed below 10^{-4} , as shown in Fig 4. This performance

is attained at the cost of a moderate increase in gate duration.

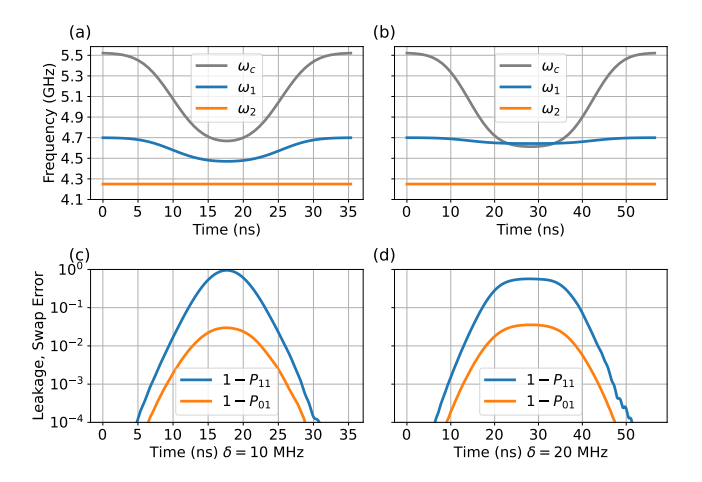


FIG. 4. (a) Control waveform for the CZ gate at $\delta/2\pi=10$ MHz. The corresponding leakage and swap errors are shown in (c). (b) Control waveform for the CZ gate at $\delta/2\pi=20$ MHz. The errors are shown in (d). An error below 10^{-4} is still achieved, albeit with an increased gate duration compared to the ideal case ($\delta=0$) in Fig. 3.

In practice, the presence of spectator qubits is a welldocumented source of infidelity in quantum gate operations, primarily mediated by residual interactions. To quantitatively evaluate the effect of spectator qubits, we employ a four-qubit grid architecture in which a CZ gate is performed on two active qubits, while the two spectator gubits are prepared in each of the computational basis states $|00\rangle$, $|01\rangle$, $|10\rangle$, and $|11\rangle$. As shown in Fig. 5a, the CZ gate is implemented between the gate qubits (Q1, Q2) by frequency tuning of Q1 and C1, while the spectator gubits (S1, S2) and the other couplers are maintained at their idle points. Numerical simulations show that maintaining the coupler between spectator and gate qubits at its idle point allows the CZ gate to consistently achieve an error rate on the order of 10^{-4} . The fidelity of the gate under each spectator configuration is detailed in Fig. 5(b). These results highlight the scheme's potential, presenting it as a promising alternative for integration into future scalable quantum processors.

V. CONCLUSIONS

This work presents a fast and high-fidelity implementation of the CZ gate based on a superconducting circuit architecture featuring energy-level-engineered qubits and a tunable coupler. The proposed scheme overcomes the speed limitation of conventional approaches by designing a resonant coupling condition through complementary anharmonicities of a Transmon and an IST qubit. This design enhances the effective qubit-qubit coupling from $\sqrt{2}g$ to 2g, significantly reducing the duration of gate.

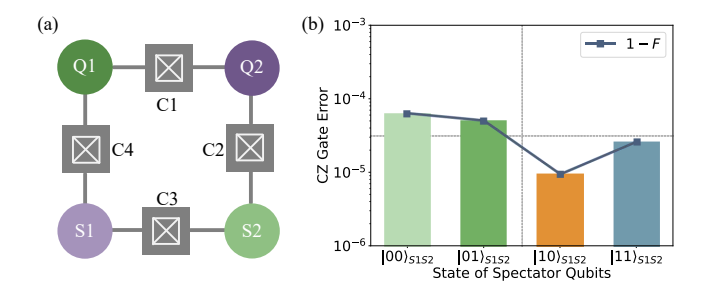


FIG. 5. (a) Four-qubit lattice configuration. Qubits Q_1 and Q_2 are used to implement the CZ gate, while S_1 and S_2 serve as spectator qubits. The full quantum state of the system is denoted as $\mid Q_1, Q_2, S_1, S_2, C_1, C_2, C_3, C_4 \rangle$, where $C_1 - C_4$ represent tunable couplers. (b) CZ gate error under different spectator qubit states. When qubits S_1 and S_2 are initialized in states $|00\rangle, |01\rangle, |10\rangle$, and $|11\rangle$, the CZ gate error between Q_1 and Q_2 remains below 10^{-4} in all cases.

Comprehensive numerical simulations demonstrate that the optimized CZ gate achieves 99.99% fidelity within 17 ns, while maintaining error rates below 10^{-4} under practical non-idealities including anharmonicity offsets and spectator qubit interactions. These results show a scalable pathway toward high-performance quantum gates compatible with large-scale quantum processors.

ACKNOWLEDGMENTS

We are grateful to Dr. Peng Zhao from the Quantum Science Center of Guangdong-Hong Kong-Macau Greater Bay Area for his guidance on circuit design, and to Dr. Ji Chu from the Shenzhen Institute for Quantum Science and Engineering for his invaluable advice on waveform optimization. We also extend our sincere thanks to Dr. Mengru Yun from Zhengzhou University for her insightful suggestions on this research scheme.

Appendix A: Circuit Hamiltonian

Fig. 1(a) shows the superconducting circuit model of a Transmon qubit and IST qubit coupled to a tunable coupler. The self-capacitance and Josephson junction energy of qubits/coupler are denoted by C_i , and $E_{J,i}$ where i = 1, c. $E_{J,1}$ and $E_{J,c}$ are tunable Josephson energy,

$$E_{J,i} = E_{J_{i,\Sigma}} \sqrt{\cos^2\left(\frac{\pi\Phi_{e,i}}{\Phi_0}\right) + d_i^2 \sin^2\left(\frac{\pi\Phi_{e,i}}{\Phi_0}\right)},$$
 (A1)

where $\Phi_0 = h/2e$ is the flux quantum, $E_{J_{i,\Sigma}} = E_{J_{i,L}} + E_{J_{i,R}}$ is the sum of Josephson energies, $d_i = (E_{J_{i,L}} - E_{J_{i,R}})/(E_{J_{i,L}} + E_{J_{i,R}})$ is the junction asymmetry. The

Lagrangian of the system can be written as L = T - U, where T and U denote the kinetic energy and the potential energy, respectively.

$$T = \frac{1}{2} [C_1 \dot{\phi}_1^2 + C_c \dot{\phi}_c^2 + C_2 \dot{\phi}_2^2 + C_{1c} (\dot{\phi}_1 - \dot{\phi}_c)^2 + C_{2c} (\dot{\phi}_2 - \dot{\phi}_c)^2 + C_{12} (\dot{\phi}_1 - \dot{\phi}_2)^2], \tag{A2}$$

$$U = E_{J,1}\cos(\varphi_1) + E_{J,c}\cos(\varphi_c) + E_{J,2}\cos(\varphi_2 + 2\pi\phi_{ext}) + \frac{1}{2}E_L\varphi_2^2,$$
(A3)

The full system Hamiltonian is

$$H = \sum_{\varphi_i} \dot{\varphi}_i \frac{\partial L}{\partial \dot{\varphi}_i} - L = \sum_{i=1,2,c} H_i + \sum_{i,j=1,2,c}^{i < j} H_{ij}, \quad (A4)$$

The Hamiltonians for the Transmon qubit and the coupler are denoted by H_1 and H_c , respectively.

$$H_1 = \frac{1}{2} (\frac{1}{2e})^2 C_1 \dot{\varphi}_1^2 - E_{J,1} \cos(\varphi_1)$$

= $4E_{C,1} n_1^2 - E_{J,1} \cos(\varphi_1)$, (A5)

$$H_c = 4E_{C,c}n_c^2 - E_{J,c}\cos(\varphi_c). \tag{A6}$$

 H_2 is the Hamiltonian of IST qubit,

$$H_2 = 4E_{C,2}n_2^2 - E_{J2}\cos(\varphi_2 + 2\pi\phi_{\text{ext}}) + \frac{1}{2}E_L\varphi_L^2$$
, (A7)

where E_{J2} and E_L can be expressed through the equivalent inductances of the junction and the linear inductor as $E_{J2} = \frac{\Phi_0^2}{4\pi^2 L_{J2}}$, $E_L = \frac{\Phi_0^2}{4\pi^2 L}$. The interaction term of Hamiltonian between qubit and coupler is

$$H_{ic} = (2e)^2 \frac{C_{ic}}{C_i C_c} n_i n_c, \tag{A8}$$

and the direct interaction of qubit is

$$H_{12} = (2e)^2 \frac{C_{12} + C_{1c}C_{2c}/C_c}{C_1C_2} n_1 n_2,$$
 (A9)

We approximate the Hamiltonian of the Transmon qubit and coupler by first expanding the cosine term to leading order and then introducing the standard annihilation and creation operators for the linearized circuit.

$$H_k \approx 4E_{C,k}n_k^2 - E_{Jk} \left(1 - \frac{1}{2}\varphi_k^2 + \frac{1}{24}\varphi_k^4 \right)$$

$$\approx \omega_k a_k^{\dagger} a_k + \frac{\alpha_k}{2} a_k^{\dagger} a_k (a_k^{\dagger} a_k - 1), \tag{A10}$$

where

$$\omega_{k} = \sqrt{8E_{C,k}E_{J,k}} - E_{C,k},$$

$$\alpha_{k} = -E_{C,k},$$

$$\varphi_{k} = \left(\frac{8E_{C,k}}{E_{J,k}}\right)^{1/4} \frac{a_{k} + a_{k}^{\dagger}}{\sqrt{2}},$$

$$n_{k} = \left(\frac{8E_{C,k}}{E_{J,k}}\right)^{-1/4} \frac{a_{k} - a_{k}^{\dagger}}{i\sqrt{2}},$$
(A11)

with k=1,c. We are interested in the regime of a weak inductive shunt with $E_L > E_{J2}$, leading to a strong harmonic confinement and therefore to a single-well phase potential (as opposed to the typical corrugated phase potential of the $E_L << E_{J2}$ limit). In the half flux quantum $\phi_{\rm ext} = 0.5$, the IST Hamiltonian can be approximately given by

$$H_{2} \approx 4E_{C,2}n_{2}^{2} + \frac{1}{2}(E_{L} - E_{J,2})\varphi_{2}^{2} + \frac{1}{24}E_{J,2}\varphi_{2}^{4}$$

$$\approx \omega_{2}a_{2}^{\dagger}a_{2} + \frac{\alpha_{2}}{2}a_{2}^{\dagger}a_{2}(a_{2}^{\dagger}a_{2} - 1), \tag{A12}$$

where

$$\omega_{2} = \sqrt{8E_{C,2} (E_{L} - E_{J,2})} + \frac{E_{C,2}E_{J2}}{E_{L} - E_{J2}},$$

$$\alpha_{2} = \frac{E_{C,2}}{2} \frac{E_{J}}{E_{L} - E_{J,2}},$$

$$\varphi_{2} = \left(\frac{8E_{C,2}}{E_{L} - E_{J,2}}\right)^{1/4} \frac{a_{2} + a_{2}^{\dagger}}{\sqrt{2}},$$

$$n_{2} = \left(\frac{8E_{C,2}}{E_{L} - E_{J,2}}\right)^{-1/4} \frac{a_{2} - a_{2}^{\dagger}}{i\sqrt{2}}.$$
(A13)

The inter-qubit coupling can be described as

$$H_{12} = g_{12} \left(a_1^{\dagger} a_2 + a_1 a_2^{\dagger} - a_1 a_2 - a_1^{\dagger} a_2^{\dagger} \right),$$

$$g_{12} = -(2e)^2 \frac{C_{12} + C_{1c} C_{2c} / C_c}{2C_1 C_2} \left(\frac{8E_{C,2}}{E_L - E_{J,2}} \frac{8E_{C,1}}{E_{J,1}} \right)^{-\frac{1}{4}}.$$
(A14)

The coupling of qubit-coupler are

$$H_{1c} = g_{1c}(a_1^{\dagger}a_c + a_1a_c^{\dagger} - a_1a_c - a_1^{\dagger}a_c^{\dagger}),$$

$$H_{1c} = g_{2c}(a_2^{\dagger}a_c + a_2a_c^{\dagger} - a_2a_c - a_2^{\dagger}a_c^{\dagger}),$$

$$g_{1c} = -(2e)^2 \frac{C_{1c}}{2C_1C_c} \left(\frac{8E_{C,1}}{E_{J,1}} \frac{8E_{C,c}}{E_{J,c}}\right)^{-\frac{1}{4}},$$

$$g_{2c} = -(2e)^2 \frac{C_{2c}}{2C_2C_c} \left(\frac{8E_{C,2}}{E_{L} - E_{L2}} \frac{8E_{C,c}}{E_{Lc}}\right)^{-\frac{1}{4}}.$$
(A15)

Therefore the full Hamiltonian of system has following form:

$$\hat{H}/\hbar = \sum_{i=1,2,c} \left(\omega_i \hat{a}_i^{\dagger} \hat{a}_i + \frac{\alpha_i}{2} \hat{a}_i^{\dagger} \hat{a}_i^{\dagger} \hat{a}_i \hat{a}_i \right) + \sum_{i < j} g_{ij} \left(\hat{a}_i^{\dagger} \hat{a}_j + \hat{a}_i \hat{a}_j^{\dagger} - \hat{a}_i \hat{a}_j - \hat{a}_i^{\dagger} \hat{a}_j^{\dagger} \right).$$
(A16)

R. Acharya, D. A. Abanin, L. Aghababaie-Beni, I. Aleiner, T. I. Andersen, M. Ansmann, F. Arute, K. Arya, A. Asfaw, N. Astrakhantsev, et al., Quantum error correction below the surface code threshold, Nature (2024).

Appendix B: Cost Function

This appendix defines the cost function used to optimize the parameters of the CZ gate. The goal is to identify the experimental parameter set $\vec{p} = (t_{\text{hold}}, \omega_c^{on}, \omega_q^{on})$ that yields a quantum operation closest to the ideal CZ gate. The proximity to the ideal gate is quantified by a cost function, $C(\vec{p})$, which incorporates two primary error sources: an incorrect conditional phase and leakage out of the computational subspace. The total cost function is defined as the sum of these two error terms:

$$C(\vec{p}) = C_{\text{phase}}(\vec{p}) + C_{\text{leak}}(\vec{p}). \tag{B1}$$

The ideal CZ gate imparts a phase of π exclusively to the $|11\rangle$ computational basis state. For a given set of parameters \vec{p} , the simulated evolution yields a final state for each basis state. The actual conditional phase, $\theta(\vec{p})$, is extracted from the system's evolution as:

$$\theta(\vec{p}) = \arg \langle \psi_{\scriptscriptstyle 11} | \psi_{\scriptscriptstyle f} \rangle - \arg \langle \psi_{\scriptscriptstyle 01} | \psi_{\scriptscriptstyle f} \rangle - \arg \langle \psi_{\scriptscriptstyle 10} | \psi_{\scriptscriptstyle f} \rangle + \arg \langle \psi_{\scriptscriptstyle 00} | \psi_{\scriptscriptstyle f} \rangle, \tag{B2}$$

where $|\psi_f\rangle$ is the final state obtained from evolving the initial state $\sum_{j,k=0,1} \alpha_{jk} | jk \rangle$. The phase error is then defined as the squared deviation from the target value

$$C_{\text{phase}}(\vec{p}) = (|\theta(\vec{p})| - \pi)^2. \tag{B3}$$

Leakage into non-computational states is a critical source of infidelity. The leakage error is defined as the total population outside the two-qubit computational basis subspace $\{|00\rangle, |01\rangle, |10\rangle, |11\rangle\}$ after the gate operation, averaged over the computational basis states. It is given by

$$C_{\text{leak}}(\vec{p}) = 1 - \sum_{j,k=0,1} \alpha_{jk} \langle \psi_f | ij \rangle.$$
 (B4)

The optimal parameter $\vec{p}_{\rm opt}$ are found by numerically minimizing the total cost:

$$\vec{p}_{\text{opt}} = \underset{\vec{p}}{\operatorname{arg\,min}} \{ C(\vec{p}) \}.$$
 (B5)

This minimization is performed using a gradient-free algorithm (e.g., Nelder-Mead), which is robust for a low-dimensional parameter space. The numerical simulations of the system's time evolution under the parameterized control pulses were conducted using the QuTiP package [32].

^[2] P. V. Klimov, A. Bengtsson, C. Quintana, A. Bourassa, S. Hong, A. Dunsworth, K. J. Satzinger, W. P. Livingston, V. Sivak, M. Y. Niu, et al., Optimizing quantum gates towards the scale of logical qubits, Nature Communications 15, 2442 (2024).

- [3] A. Gyenis, P. S. Mundada, A. Di Paolo, T. M. Hazard, X. You, D. I. Schuster, J. Koch, A. Blais, and A. A. Houck, Experimental realization of a protected superconducting circuit derived from the 0-π qubit, PRX Quantum 2, 010339 (2021).
- [4] A. Gyenis, A. Di Paolo, J. Koch, A. Blais, A. A. Houck, and D. I. Schuster, Moving beyond the transmon: Noiseprotected superconducting quantum circuits, PRX Quantum 2, 030101 (2021).
- [5] I. Siddiqi, Engineering high-coherence superconducting qubits, Nature Reviews Materials 6, 875 (2021).
- [6] F. Hassani, M. Peruzzo, L. Kapoor, A. Trioni, M. Zemlicka, and J. M. Fink, Inductively shunted transmons exhibit noise insensitive plasmon states and a fluxon decay exceeding 3 hours, Nature Communications 14, 3968 (2023).
- [7] A. Somoroff, Q. Ficheux, R. A. Mencia, H. Xiong, R. Kuzmin, and V. E. Manucharyan, Millisecond coherence in a superconducting qubit, Physical Review Letters 130, 267001 (2023).
- [8] A. P. Place, L. V. Rodgers, P. Mundada, B. M. Smitham, M. Fitzpatrick, Z. Leng, A. Premkumar, J. Bryon, A. Vrajitoarea, S. Sussman, et al., New material platform for superconducting transmon qubits with coherence times exceeding 0.3 milliseconds, Nature communications 12, 1779 (2021).
- [9] C. Wang, X. Li, H. Xu, Z. Li, J. Wang, Z. Yang, Z. Mi, X. Liang, T. Su, C. Yang, et al., Towards practical quantum computers: Transmon qubit with a lifetime approaching 0.5 milliseconds, npj Quantum Information 8, 3 (2022).
- [10] S. Ganjam, Y. Wang, Y. Lu, A. Banerjee, C. U. Lei, L. Krayzman, K. Kisslinger, C. Zhou, R. Li, Y. Jia, et al., Surpassing millisecond coherence in on chip superconducting quantum memories by optimizing materials and circuit design, Nature Communications 15, 3687 (2024).
- [11] J. Verjauw, R. Acharya, J. Van Damme, T. Ivanov, D. P. Lozano, F. Mohiyaddin, D. Wan, J. Jussot, A. Vadiraj, M. Mongillo, et al., Path toward manufacturable superconducting qubits with relaxation times exceeding 0.1 ms, npj Quantum Information 8, 93 (2022).
- [12] S. Kim, H. Terai, T. Yamashita, W. Qiu, T. Fuse, F. Yoshihara, S. Ashhab, K. Inomata, and K. Semba, Enhanced coherence of all-nitride superconducting qubits epitaxially grown on silicon substrate, Communications Materials 2, 98 (2021).
- [13] M. P. Bland, F. Bahrami, J. G. Martinez, P. H. Preste-gaard, B. M. Smitham, A. Joshi, E. Hedrick, A. Pakpour-Tabrizi, S. Kumar, A. Jindal, et al., 2d transmons with lifetimes and coherence times exceeding 1 millisecond, arXiv preprint arXiv:2503.14798 (2025).
- [14] J. M. Martinis and M. R. Geller, Fast adiabatic qubit gates using only σ z control, Physical Review A **90**, 022307 (2014).
- [15] Y. Xu, J. Chu, J. Yuan, J. Qiu, Y. Zhou, L. Zhang, X. Tan, Y. Yu, S. Liu, J. Li, et al., High-fidelity, highscalability two-qubit gate scheme for superconducting qubits, Physical review letters 125, 240503 (2020).
- [16] J. Chu and F. Yan, Coupler-assisted controlled-phase gate with enhanced adiabaticity, Physical Review Applied 16, 054020 (2021).
- [17] Y. Sung, L. Ding, J. Braumüller, A. Vepsäläinen, B. Kannan, M. Kjaergaard, A. Greene, G. O. Samach, C. Mc-

- Nally, D. Kim, $et\ al.$, Realization of high-fidelity cz and zz-free iswap gates with a tunable coupler, Physical Review X 11, 021058 (2021).
- [18] R. Barends, C. Quintana, A. Petukhov, Y. Chen, D. Kafri, K. Kechedzhi, R. Collins, O. Naaman, S. Boixo, F. Arute, et al., Diabatic gates for frequency-tunable superconducting qubits, Physical review letters 123, 210501 (2019).
- [19] S. Li, J. Clark, S. Wang, Y. Wu, M. Gong, Z. Yan, H. Rong, H. Deng, C. Zha, C. Guo, et al., Realisation of high-fidelity nonadiabatic cz gates with superconducting qubits, npj Quantum Information 5, 84 (2019).
- [20] H. Goto, Double-transmon coupler: Fast two-qubit gate with no residual coupling for highly detuned superconducting qubits, Physical review applied 18, 034038 (2022).
- [21] R. Li, K. Kubo, Y. Ho, Z. Yan, Y. Nakamura, and H. Goto, Realization of high-fidelity cz gate based on a double-transmon coupler, Physical Review X 14, 041050 (2024).
- [22] Z. Huang, T. Kim, T. Roy, Y. Lu, A. Romanenko, S. Zhu, and A. Grassellino, Fast zz-free entangling gates for superconducting qubits assisted by a driven resonator, Physical Review Applied 22, 034007 (2024).
- [23] L. Jiang, P. Xu, S. Wu, J.-A. Sun, and F.-Q. Dou, Microwave-activated two-qubit gates for fixed-coupling and fixed-frequency transmon qubits, Physical Review A 111, 032609 (2025).
- [24] P. Zhao, P. Xu, D. Lan, J. Chu, X. Tan, H. Yu, and Y. Yu, High-contrast zz interaction using superconducting qubits with opposite-sign anharmonicity, Physical Review Letters 125, 200503 (2020).
- [25] J. Ku, X. Xu, M. Brink, D. C. McKay, J. B. Hertzberg, M. H. Ansari, and B. Plourde, Suppression of unwanted zz interactions in a hybrid two-qubit system, Physical review letters 125, 200504 (2020).
- [26] X. Xu and M. Ansari, Zz freedom in two-qubit gates, Physical review applied 15, 064074 (2021).
- [27] S. Krinner, S. Lazar, A. Remm, C. K. Andersen, N. Lacroix, G. J. Norris, C. Hellings, M. Gabureac, C. Eichler, and A. Wallraff, Benchmarking coherent errors in controlled-phase gates due to spectator qubits, Physical Review Applied 14, 024042 (2020).
- [28] P. Zhao, K. Linghu, Z. Li, P. Xu, R. Wang, G. Xue, Y. Jin, and H. Yu, Quantum crosstalk analysis for simultaneous gate operations on superconducting qubits, PRX quantum 3, 020301 (2022).
- [29] S. D. Fasciati, B. Shteynas, G. Campanaro, M. Bakr, S. Cao, V. Chidambaram, J. Wills, and P. J. Leek, Complementing the transmon by integrating a geometric shunt inductor, arXiv preprint arXiv:2410.10416 (2024).
- [30] F. Yan, P. Krantz, Y. Sung, M. Kjaergaard, D. L. Campbell, T. P. Orlando, S. Gustavsson, and W. D. Oliver, Tunable coupling scheme for implementing high-fidelity two-qubit gates, Physical Review Applied 10, 054062 (2018).
- [31] L. H. Pedersen, N. M. Møller, and K. Mølmer, Fidelity of quantum operations, Physics Letters A 367, 47 (2007).
- [32] N. Lambert, E. Giguère, P. Menczel, B. Li, P. Hopf, G. Suárez, M. Gali, J. Lishman, R. Gadhvi, R. Agarwal, et al., Qutip 5: The quantum toolbox in python, arXiv preprint arXiv:2412.04705 (2024).